

## High resolution X-ray analysis of two mutants of a curaremimetic snake toxin

Jean-François Gaucher<sup>1,\*</sup>, Renée Ménez<sup>2</sup>, Bernadette Arnoux<sup>1</sup>, Jacques Pusset<sup>2</sup> and Arnaud Ducruix<sup>1</sup>

<sup>1</sup>Laboratoire d'Enzymologie et de Biochimie Structurales, UPR 9063 CNRS, 91198 Gif-sur-Yvette, France; <sup>2</sup>Département d'Ingénierie et d'Etudes des Protéines, DSV, CE Saclay, 91191 Gif-sur-Yvette, France

A previous mutational analysis of erabutoxin a (Ea), a curaremimetic toxin from sea snake venom, showed that the substitutions S8G and S8T caused, respectively, 176-fold and 780-fold affinity decreases for the nicotinic acetylcholine receptor (AChR). In view of the fact that the side-chain of Ser8 is buried in the wild-type toxin, we wondered whether these affinity changes reflect a direct binding contribution of S8 to the receptor and/or conformational changes that could have occurred in Ea as a result of the introduced mutations. To approach this question, we solved X-ray structures of the two mutants S8G and S8T at high resolution (0.18 nm and 0.17 nm, with R factors of 18.0% and 17.9%, respectively). The data show that none of the mutations significantly modified the toxin structure. Even within the site where the toxin binds to the receptor the backbone conformation remained unchanged. Therefore, the low affinities of the mutants S8T and S8G cannot be explained by a large conformational change of the toxin structure. Although we cannot exclude the possibility that undetectable structural changes have occurred in the toxin mutants, our data support the view that, although buried between loop I and II, S8 is part of the functional epitope of the toxin.

**Keywords:** curaremimetic toxins; nicotinic acetylcholine receptor; X-ray structure.

Mutational analyses are widely used to identify the functional surfaces of proteins and to determine the contribution of interacting residues to the energetic stabilization of protein–protein complexes [1,2]. In most cases, it is assumed that the introduced mutations have little, if any, effect on the protein conformation, leading authors to conclude that affinity decreases occurring as a result of mutations are likely to reflect a direct contribution of the mutated residue to protein interaction [3]. In general, this conclusion appears to be correct, especially when it is supported by crystallographic data that indicate that the mutated residue establishes contacts with the interacting partner [3,4]. However, the situation may be more complex, as some mutations cause affinity decreases even though the mutated residue is not in the region contacting the receptor [4]. Therefore, in the absence of information regarding the three-dimensional structure of a protein–protein complex, the effect of some mutations should be considered with caution, the introduced mutation causing possibly local or even more global conformational changes in the protein. One way to tentatively clarify a doubtful case consists of elucidating the three-dimensional structure of the mutant and comparing it

with that of the wild-type protein. This situation has been met with mutations introduced at position 8 of erabutoxin a (Ea), a snake curaremimetic toxin, the functional site of which has been identified on the basis of extensive mutational analyses [5,6].

Ea is a small protein of 62 amino acids that belongs to the family of short-chain curaremimetic toxins [7], which bind to the nicotinic acetylcholine receptor (AChR) from *Torpedo marmorata* with high affinity ( $K_d = 70$  pM) and great specificity. The three-dimensional structure of Ea (Fig. 1) was elucidated by X-ray crystallography [8], revealing that its backbone is folded into three adjacent loops, rich in  $\beta$ -pleated sheet emerging from a small globular core that contains the four disulfide bridges of the toxin. The other members of the family of snake short-chain toxins adopt the same overall architecture [9–13]. With the view to identify the functional site of Ea, its cDNA has been previously cloned and expressed in *Escherichia coli* as a fusion protein [14], which was then cleaved [15]. The resulting recombinant toxin was indistinguishable from the snake toxin regarding both its biological activity [15] and its three-dimensional structure [16]. Using this expression system, a large panel of Ea mutants has been produced and used to identify the residues by which the toxin binds to both AChR [5,6] and an AChR-mimicking antibody [17]. Affinity decreases larger than 10-fold were observed when at least one type of mutation was introduced at Q7, S8, Q10, K27, W29, D31, R33, E38 and K47. Furthermore, a substantial affinity increase was observed upon mutation of I36 into arginine [6]. These 10 mutation-sensitive positions offered a plausible homogeneous surface by which Ea may interact with AChR. Of these, however, the case of Ser8 could not be interpreted as easily as the others, for the following reasons. First, the side-chain of Ser8 is partially buried in a small groove formed between loops I and II. Second, its side-chain lies approximately within the plane of the  $\beta$ -sheet and is therefore oriented differently, as

Correspondence to R. Ménez, Département d'Ingénierie et d'Etudes des Protéines, DSV, CE Saclay, 91191 Gif sur Yvette Cedex, France.

Fax: + 33 1 69 08 90 71, Tel.: + 33 1 69 08 89 66,

E-mail: rmenez@balthazar.saclay cea.fr

Abbreviations: Ea, erabutoxin a; Eb, erabutoxin b; AChR, nicotinic acetylcholine receptor.

\*Present address: EP2075 CNRS, Faculté de Pharmacie de l'Université Paris-V, France.

Note: the atomic coordinates and related structure factors for Ea S8G and Ea S8T crystal structures have been deposited with the RCSB Protein Data Bank (file names 2era and 3era, respectively).

(Received 26 March 1999, revised 23 November 1999, accepted 14 December 1999)

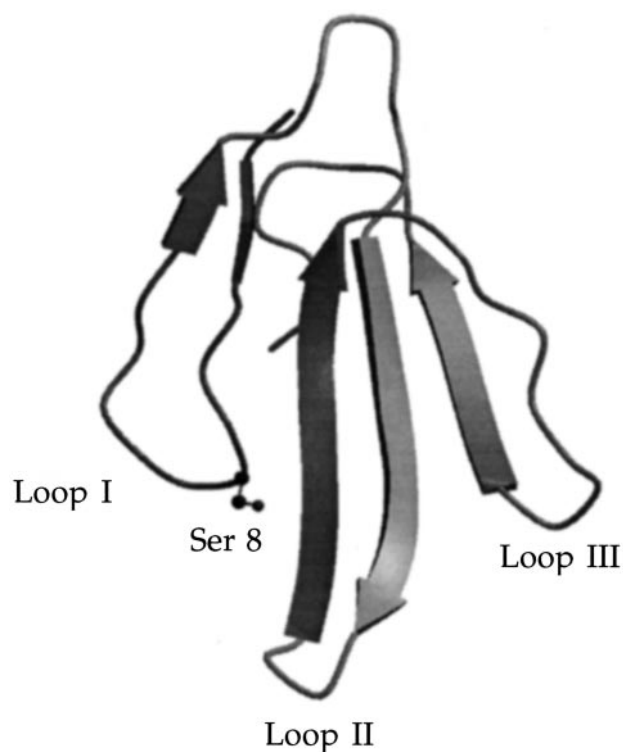


Fig. 1. Backbone representation of Ea, showing secondary structure elements. Ser8 is shown in ball-and-stick representation.

compared to those of other functional residues whose side-chains point in a direction approximately perpendicular to the plane of the  $\beta$ -sheet, toward the convex face of the toxin. Third, although the presence of Ser/Thr in homologous proteins is often considered as conservative substitution, it was striking that the S8T mutation caused the largest affinity decrease ever observed during the extensive mutational analysis of Ea [6]. Finally, preliminary data based on circular dichroism analysis of the S8G mutant suggested the possibility of slight changes in toxin secondary structure [5]. Therefore, it was anticipated that S8 could play a structural role, possibly stabilizing an appropriate proximity between loops I and II of the toxin, which both contain functionally critical residues.

In the present work we will compare the two crystal structures of mutants EaS8G and EaS8T to the three-dimensional structure of native Ea [8] and discuss the results in the frame of the implication of residue S8 in the stabilization of the toxin–AChR complex.

## MATERIALS AND METHODS

### Production, purification and characterization of the mutants

Recombinant Ea S8G and S8T mutants were expressed in bacterial host *E. coli* and purified as previously described [5,6,9]. Amino-acid analysis, sequencing and isoelectric focusing of the mutants were performed. The molar absorbance value at 278 nm was determined by measuring the absorbance at this wavelength of a given solution of mutant and the corresponding protein concentration as determined by amino acid analysis [ $A_{278\text{nm}}(\text{Ea S8T}) = A_{278\text{nm}}(\text{Ea S8G}) = 9000 \pm 50 \text{ M}^{-1} \cdot \text{cm}^{-1}$ ].

### Dichroic spectra

Each sample was dissolved in water, and acidic or alkaline pH were obtained by addition of HCl or  $\text{NH}_4\text{OH}$ . Dichroic spectra were recorded at 22 °C using a CD6 Jobin Yvon dichrograph. The CD of each sample was measured in 0.02 cm length cells from 280–180 nm, with a total absorbance less than 1.0 to ensure sufficient light transmission. The data were collected using an on-line PC computer and at least 10 spectra for each sample were averaged and corrected by subtraction of solvent spectra.

### Crystallization of mutants

The crystallization experiments were performed at 18 °C using vapor diffusion in Linbro tissue culture plates. It has been shown that depending on the nature of a given salt, the solubility and crystallization properties are profoundly affected [18]. For this reason and because Ea and Ea mutants are basic proteins ( $\text{pI} = 9.68$ ), reverse Hofmeister series were tested. For both mutants, hanging drops of 4  $\mu\text{L}$  (2  $\mu\text{L}$  of 7 mM toxin solution in water and 2  $\mu\text{L}$  of the reservoir solution) were equilibrated against 1 mL reservoir containing the crystallizing agent in a buffer.

*Ea S8G.* Four different reservoir solutions lead to crystals: 50 mM NaOAc pH 4.5 in 250 mM NaSCN; 50 mM NaOAc pH 4.5 in 3 M NaCl; 11 mM Tris/HCl pH 9.4 in 300 mM  $\text{Na}_2\text{SO}_4$ ; 11 mM Tris/HCl pH 9.4 in 1 M  $(\text{NH}_4)_2\text{SO}_4$ . The best crystals were obtained using NaCl as crystallizing agent. They belong to the  $\text{P}2_12_12_1$  space group with unit cell parameters  $a = 4.95 \text{ nm}$ ,  $b = 4.64 \text{ nm}$ ,  $c = 2.17 \text{ nm}$  and one molecule per asymmetric unit. They are isomorphous with wild-type Ea (PDB entry 5ebx) and Eb (PDB entry 3ebx) previously published [8,9].

*Ea S8T.* Only one condition led to crystallization: a hanging drop was equilibrated against a reservoir containing 210 mM NaSCN in 50 mM NaOAc buffer (pH 4.5). After one week, NaSCN concentration of the reservoir was gradually increased by 10 mM until reaching 320 mM at which concentration crystals appeared. They belong to the  $\text{P}2_12_12_1$  space group with unit cell parameters  $a = 5.54 \text{ nm}$ ,  $b = 5.30 \text{ nm}$ ,  $c = 4.05 \text{ nm}$  and two molecules per asymmetric unit. They are isomorphous with wild-type Eb crystallized in similar conditions (PDB entry 6ebx) [19].

### Diffraction data collection and processing

Data of Ea S8T and Ea S8G were collected on W32 synchrotron beam line [20] at LURE, Orsay (France) at a wavelength of  $\lambda = 0.0901 \text{ nm}$ , using a Mar-research image plate detector. In both cases, the crystal to film distance was 160 mm and one crystal of each mutant was sufficient to collect complete data sets. Details of data collections are shown in Table 1.

X-ray data were processed with MOSFLM software [21] and reduced using ROTAVATA and AGROVATA programs from the CCP4 suite [22].

### Structure refinement

Table 2 shows the final structure refinement statistics.

*Ea S8G.* The orientation and location of the Ea S8G mutant molecule were checked by rigid-body refinement at 0.3 nm resolution, using coordinates from the recombinant Ea structure

**Table 1. Statistics on data collection.**

	Ea S8G	Ea S8T
Crystal size	100 × 100 × 300 μm	80 × 80 × 400 μm
Diffraction limit	1.7–0.18 nm	1.0–0.17 nm
No. observed reflection	41 373	46 741
No. unique reflection	4924	13 852
R <sub>sym</sub> (whole set)	4.7%	6.9%
I/σ (whole set)	13.0	7.7
Completeness (whole set)	99.0%	97.8%
R <sub>sym</sub> (outer shell)	11.6%	20.5%
I/σ (outer shell)	6.3	3.4
Completeness (outer shell)	97.0%	97.3%

[16]. Refinement was done using the XPLOR program [23]. After a first set of refinement and a step by step increase of resolution to 0.22 nm, a difference Fourier map showed without ambiguity the S8G mutation (R-factor 29.2%, R<sub>free</sub> 41.1% [24]). The refinement was extended to 0.20 nm with overall B-factor refinement. A simulated annealing procedure (2000–300°K) was applied, and finally individual atomic B-factors were introduced and refined (R-factor 25.4%, R<sub>free</sub> 32.4%). 61 water molecules were added using the restraint ARP procedure [25] (R-factor 18.3%, R<sub>free</sub> 23.6%). All data were used for the final refinement cycle (final R-factor 18.0%, = 1.0–0.18 nm,  $F > 2\sigma$ ).

*Ea S8T.* Refinement was started by molecular replacement [26] and rigid-body procedures using the Ea S8G structure [= 1–0.3 nm, R-factor 42.4%, R<sub>free</sub> 41.4% (10% of data)]. The two molecules of the asymmetric unit were refined independently by energy minimization, slow cooling procedure and overall B-factor refinement (= 1–0.2 nm, R-factor 25.4%, R<sub>free</sub> 31.0%). At this step, a Fourier difference map showed in the Gly8 vicinity of each molecule of the asymmetric unit an electronic density corresponding to a threonine with a well defined orientation. After substituting a threonine at position 8, the refinement was extended to 0.19 nm with individual atomic B-factor refinement. A restraint ARP procedure [25] was used to introduce 118 water molecules, three of which proved to be thiocyanate ions defined by a well shaped electronic density in the 2Fo-Fc map (= 1–0.16 nm, R-factor 20.0%, R<sub>free</sub> 22.0%); one of them has already been described in the isomorphous structure of Eb (6ebx) [19]. Six alternative side-chain conformations were next introduced, before the final cycle of refinement using the complete data set (final R-factor 17.9%, = 1–0.17 nm,  $F > 2\sigma$ ).

The structures of Ea S8G and Ea S8T were determined at high resolution, with a good geometry according to the analysis parameters calculated with PROCHECK v3.0 algorithm [27]. Estimation of main error on the coordinates from a  $\sigma_a$  plot [28] gives 0.011 nm for Ea S8G and 0.022 nm for Ea S8T.

## RESULTS

### Measurement of far UV dichroism of Ea S8G and Ea S8T

Spectra obtained for Ea S8G and Ea S8T at pH 4.5 display a negative trough at 215 nm and a positive band at 197 nm indicating that the overall secondary structure of proteins is predominantly organized into  $\beta$  structure. The positive band at 228 nm reflects the contribution of the aromatic residues Thr25

and Trp29 [29]. They are similar to Ea and Eb spectra (Fig. 2), suggesting that the secondary structure of the toxin is not affected by S8 mutations. The variation of molar ellipticity at 228 nm as a function of pH for Ea mutants shows that denaturation of toxins occurs between pH 3.4 and 2.3 (data not shown), in agreement with previous CD spectra [30] and NMR data for Eb [31].

### X-ray structures of Ea S8G and Ea S8T

In order to estimate the effect of the mutations on the secondary structure of the protein, we have calculated the rmsd of backbone positions for all available X-ray structures of erabutoxin (Table 4). Both mutants have structures very close to wild-type Ea and Eb, but as shown in Table 3 non-isomorphous structures have higher rmsds than isomorphous ones. It is worth mentioning that the H26N mutation, which distinguishes Ea from Eb, has no effect on the overall protein conformation [8]. Consequently, in order to discriminate between the effects of point mutation of the toxin and packing, we have compared each mutant with the isomorphous wild-type Ea or Eb structure.

*Ea S8G.* The Ea S8G backbone deviates by more than one rmsd

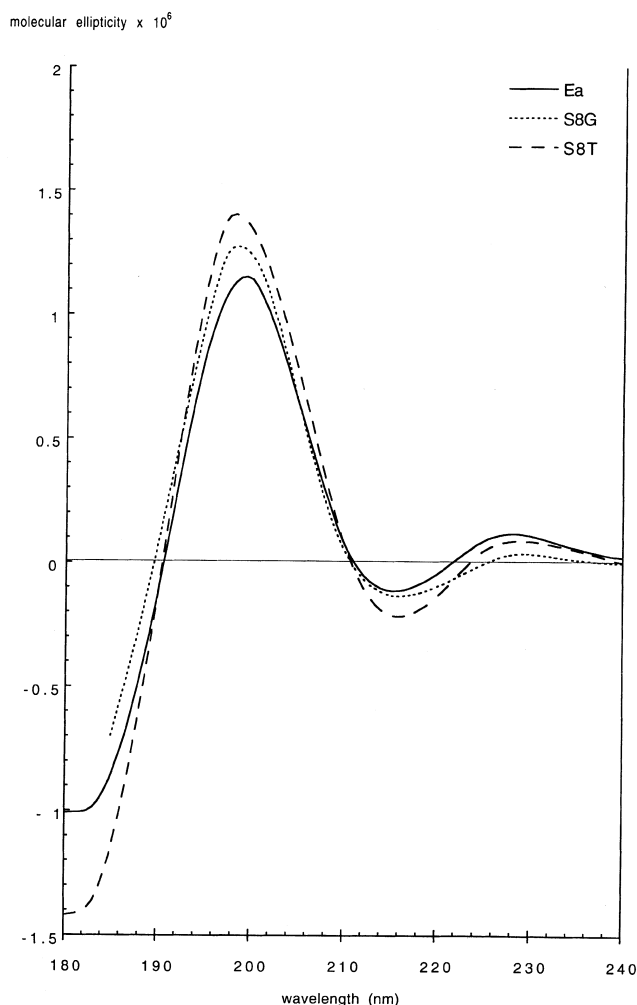


**Fig. 2.** Far UV CD spectra of native Ea and recombinant Ea S8G and Ea S8T. For each spectrum, protein concentration was  $10^{-4}$  M, cell path length 0.02 cm and temperature 22 °C.

**Table 2.** Statistics for the refined structures.

	Ea S8G	Ea S8T
No. of protein atoms	471	977
No. of water molecules	61	105
No. of thiocyanate ions	0	3
Resolution (nm)	0.18	0.17
Final R-factor	18.0%	17.9%
Final R <sub>free</sub>	23.6%	22.0%
Mean B factor (10 <sup>-2</sup> nm <sup>2</sup> )		
protein (all atoms)	10.3	11.3 (molecule A), 15.8 (molecule B)
backbone	8.6	10.2 (molecule A), 14.3 (molecule B)
side-chain	12.2	12.4 (molecule A), 17.3 (molecule B)
solvent	25.9	30.8
Rmsd from ideal geometry		
bond lengths (nm)	0.0008	0.0006
bond angles (°)	1.64	1.59
dihedral angles (°)	26.9	25.95
improper angles (°)	1.34	1.29
overall G factor	0.23	0.21

**Table 3.** Comparison of the backbones of crystallographic structures of Ea, Eb and Ea mutants.

Rmsd on backbone position (nm)	Ea S8G	Eb (3ebx)	Ea (5ebx)	Ea S8T (molecule A)	Eb (6ebx) (molecule A)	Ea S8T (molecule B)	Eb (6ebx) (molecule B)
Ea S8G	–	0.022 <sup>a</sup>	0.030 <sup>a</sup>	0.084 <sup>b</sup>	0.082 <sup>b</sup>	0.082 <sup>b</sup>	0.078 <sup>b</sup>
Eb (3ebx)		–	0.025 <sup>a</sup>	0.079 <sup>b</sup>	0.085 <sup>b</sup>	0.083 <sup>b</sup>	0.081 <sup>b</sup>
Ea (5ebx)			–	0.074 <sup>b</sup>	0.076 <sup>b</sup>	0.076 <sup>b</sup>	0.071 <sup>b</sup>
Ea S8T (molecule A)				–	0.023 <sup>a</sup>	0.046 <sup>c</sup>	0.045 <sup>c</sup>
Eb (6ebx; molecule A)					–	0.047 <sup>c</sup>	0.042 <sup>c</sup>
Ea S8T (molecule B)						–	0.019 <sup>a</sup>

<sup>a</sup> Isomorphous cell and same position in the asymmetric unit; <sup>b</sup> nonisomorphous cell; <sup>c</sup> isomorphous cell and different position in the asymmetric unit. Protein Data Bank entries are given in parentheses.

**Table 4.** Available Protein Data Bank structures of short neurotoxins.

Name	No. residues	Species	Method	Resolution or no. of models	R-factor or rmsd between models	PDB entries	Reference
Erabutoxin a	62	<i>L. semifasciata</i>	X-ray	0.2 nm	16.8%	5ebx	[8]
Erabutoxin b	62	<i>L. semifasciata</i>	X-ray	0.14 nm	14.0%	3ebx	[38]
Erabutoxin b	62	<i>L. semifasciata</i>	X-ray	0.17 nm	19.4%	6ebx	[19]
Erabutoxin b	62	<i>L. semifasciata</i>	NMR	14 models	0.06 nm <sup>a</sup>	1era/1fra	[31]
Toxin α	61	<i>N. nigricollis</i>	NMR	8 models	0.05 nm	1nea	[10]
α-Neurotoxin	60	<i>D. p. polylepis</i>	NMR	20 models	0.07 nm	1ntx	[39]
Neurotoxin II	61	<i>N. naja oxiana</i>	NMR	19 models	0.05 nm	1nor	[40]
Cobrotoxin II	62	<i>N. naja atra</i>	NMR	23 models	0.09 nm <sup>a</sup>	1cod/1coe	[12]

<sup>a</sup> Rmsd calculated on partial backbone.

from the isomorphous wild-type Eb (3ebx) structure at positions 9–10 (loop I), 32–33 (loop II) and 44–51 (loop III), and from the isomorphous wild-type Ea (5ebx) structure, at positions 8–12, 32–36, 45–52. The profile of averaged B-factors per residues are similar for Ea S8G and wild-type Ea or Eb crystallized with one molecule per asymmetric unit, and are not affected by the S8G mutation. In the three structures, residues with the highest B-factors are located on the third loop.

However, the S8G mutation results in a modification of the backbone conformation of residue 8 from  $\phi = 38 \pm 4^\circ$ ,  $\psi = -105 \pm 5^\circ$  in the wild types (averaged on all crystallographic models of Ea and Eb) to  $\phi = 50^\circ$ ,  $\psi = -133^\circ$ . The S8G mutation modifies the orientation of residues 8–11, which are slightly displaced by less than 0.1 nm toward the convex face of the protein as compared with the isomorphous Eb (3ebx) and Ea (5ebx) structures.

*Ea* S8T. Comparisons are made with the isomorphous Eb (6ebx) crystallized with two molecules in the asymmetric unit. Differences higher than one rmsd are observed in two regions: (a) the extremity of loop II, which forms a type I  $\beta$  turn in both molecules of *Ea* S8T, as in the nonisomorphous structures of Eb and *Ea*. This conformation differs from the nonconventional turn observed in the isomorphous 6ebx structure, which displays highest B-factors in this region. (b) The turn 18–21 of molecule A which has been rebuilt in the electron density as a  $\beta$ -turn conformation close to type I.

## DISCUSSION

The high resolution X-ray structures of the two mutants S8T and S8G helped us to better understand the role of Ser8 in the function of *Ea*. As already mentioned, the two mutations decreased the *Ea*-nAChR affinity by 176 and 780-fold, respectively, although it was not clear why this occurs. Previous structural studies on the native toxin showed that Ser8 is located at position  $i + 2$  of a  $\beta$  turn of type II' where a glycine is generally expected [32]. Its conformation is not in the favorable areas of the Ramachandran diagram [33]. Also, Ser8 is partly buried in a valley between loops I and II and lies on the flank of the convex face, whereas most residues that interact with AChR point toward the same direction, roughly perpendicular to the sheet.

### Structure of loop I from native and point mutated *Ea*

In the native *Ea* structure, residues 7–10 form a  $\beta$ -II' type turn, stabilized by an internal hydrogen bond between the Gln7 carbonyl oxygen atom and the Gln10 nitrogen atom. The partially buried Arg39 conserved in loop II of all short chain curare-mimetic toxins interacts with the carbonyl oxygen atoms of His6, Asn61 and the C terminus (Fig. 3A). These interactions are present in other snake toxins such as fasciculin [34,35] and cardiotoxin [36], where they maintain the position of the C terminus and its relative orientation to loop II and the core of the protein. In *Ea* and in other homologous short chain toxins, Arg39 constrains the turn of loop I into a  $\beta$ -II' type conformation through a strong electrostatic interaction with the Ser8 carbonyl oxygen atom, despite a steric clash between C $\beta$ 8 and N9 as shown by the short associated distance ( $d = 0.27 \pm 0.01$  nm). Thus, the hydroxyl of Ser8 is oriented toward the second loop, being hydrogen bonded to the Ile37 nitrogen.

Irrespective of the nature of the introduced mutation (S8G or S8T), a  $\beta$ -turn type II' remains present between residues 7 and

10, at the tip of loop I. The main structural consequence of the S8G mutation (Fig. 3B) is the stabilization of the  $\beta$ -II' type turn conformation due to the abolition of the short contact between C $\beta$ 8 and N9. Despite the absence of a hydrogen bond between O $\gamma$  Ser8 in loop I and N37 in the second loop, the relative position of the two loops is not modified. In the mutant S8T, the hydroxyl group of the threonine plays a comparable stabilizing role with N37, as compared to what is seen in the wild-type toxin (Fig. 3C). Therefore, the two mutations neither affected the type of turn at the tip of loop I nor the relative positions of the two loops, invalidating a major structural role of serine 8 in the local spatial organization.

### Implications for AChR binding

It was previously shown that Ser8 is part of a homogeneous surface composed of several residues functionally important for toxin binding to AChR [6]. Here we show that the mutation (S8T) that caused the largest of all affinity decreases [36] is not associated with a large conformational change. Therefore, our data suggest that the affinity decreases that take place upon mutations at position 8 reflect a direct contribution by Ser8 to receptor binding. However, in view of the peculiar position of this residue between the two toxin loops and despite the high resolution of the two structures, we cannot exclude the possibility that small and undetected structural changes have occurred upon mutation and might be responsible for the observed affinity decreases.

In the frame of the hypothesis of a functional role for Ser8 it is interesting to note that the low B-factor water molecule observed near Gly8 (Fig. 3B) might partially restore a hydrogen bond that could occur between AChR and O $\gamma$  Ser8. This water molecule ( $B = 0.13$  nm<sup>2</sup>), is sitting near the position occupied by the O $\gamma$  of Ser8 in the wild type (the H<sub>2</sub>O–O $\gamma$  distance is 0.09 nm). It simultaneously binds to the peptide nitrogen atom of Ile37, the carbonyl oxygen atom of Thr35 and another water molecule. In the S8T mutant, the Thr8 methyl  $\gamma$  might hinder binding to the AChR by steric hindrance on the convex face (Fig. 4) and cause the observed larger affinity decrease.

The major part of the *Ea* toxic site, as identified by a mutational analysis, forms a convex surface at the tips of loops I, II and III [6]. All the residues except Ser8 (Gln7, Gln10, Lys27, Trp29, Asp31, Arg33, Ile36, Glu38, Lys47) have long side-chains largely exposed to solvent and are conformationally free. As commonly observed, the X-ray structures of *Ea* and Eb, for which the unit cells differ, show different conformations for

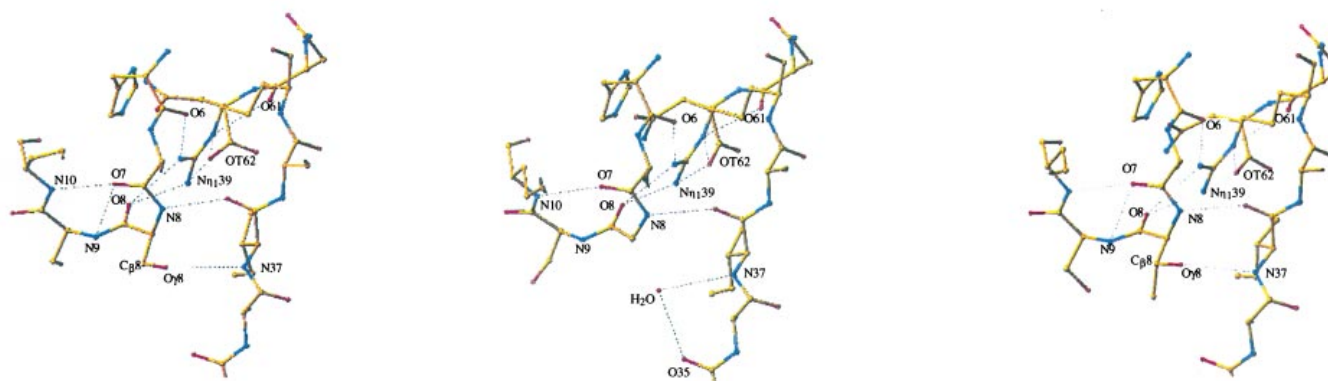
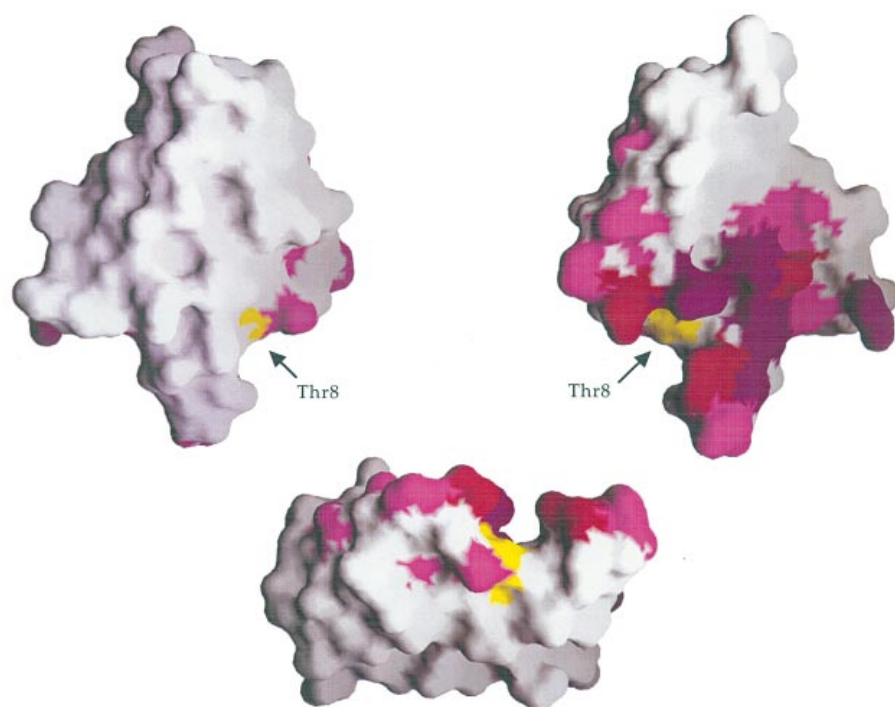


Fig. 3. Representation of the tip of loop I in three structures (A) *Ea*, (B) *EaS8G* and (C) *EaS8T*.



**Fig. 4.** Grasp views [37] of the Ea S8T molecular surface with a color code indicating mutagenesis results. Pink, mutations leading to an affinity decrease between 2 and 10; purple, between 10 and 100; red, greater than 100. Top left, convex face; top right, concave face; bottom, orthogonal view.

some of these residues as a result of crystal packing. They slightly adjust themselves to the contact surfaces, as they might do when they bind the AchR surface. To the contrary, Ser8 presents a low accessible area in the bottom of the groove between the tip of loop I and loop II, and has a short side-chain with a low B-factor and degree of freedom. The area around Ser8 might constitute a close-fitting area of contact with a receptor zone, locally sensitive to weak variation of the toxin surface topology. The Ser8 neighborhood is mostly hydrophilic and comprises several hydrogen bond donors or acceptors, the Ser9 O $\gamma$ , the Ser9 nitrogen atom and the Thr35 carbonyl oxygen atom, which point toward the solvent near Ser8 and could interact with AchR.

We wish to speculate that a S8V mutation would induce a similar extensive decrease in affinity for the AchR receptor. One methyl group of the valine would be at the same location as that of threonine whereas the other site would prevent any hydrogen bond from the site of the native serine hydroxyl group. Of course, we cannot completely exclude that a weak modification of the structure, induced by the mutation, may lead to the decreases in affinity. To definitely resolve this question the crystal structure of a toxin–receptor complex needs to be determined.

In conclusion, we have shown that the Ea S8T and Ea S8G mutants conserve the native Ea structure. We propose that Ser8, although buried and located on the convex face of the toxin, interacts directly with the AchR, which would suggest that the hydroxyl group of Ser8 is making a functionally important hydrogen bond with an acceptor from the receptor. The invariance of this residue through the short neurotoxin class may reflect the conservation of this mode of association with AchR.

## ACKNOWLEDGEMENTS

We are grateful to Prof. André Ménez for initiating this study. We thank Caroline Lemaire and Pascal Drevet for providing us with the *E. coli* culture supernatant and Françoise Bouet for performing amino acid analysis

and sequencing of the mutants. We are also indebted to LURE for providing excellent facilities and the Centre National de la Recherche Scientifique and the Centre d'Etudes Atomiques for financial support. J. F. G. was supported by Ministère de l'Éducation Nationale, de la Recherche et de la Technologie.

## REFERENCES

- Cunningham, B.C. & Wells, J.A. (1989) High-resolution epitope mapping of hGH–receptor interactions by alanine-scanning mutagenesis. *Science* **244**, 1081–1085.
- Cunningham, B.C. & Wells, J.A. (1993) Comparison of a structural and a functional epitope. *J. Mol. Biol.* **234**, 554–563. (Erratum (1994), *J. Mol. Biol.* **237**, 513.)
- Kam-Morgan, L.N., Smith-Gill, S.J., Taylor, M.G., Zhang, L., Wilson, A.C. & Kirsch, J.F. (1993) High-resolution mapping of the HyHEL-10 epitope of chicken lysozyme by site-directed mutagenesis. *Proc. Natl Acad. Sci. USA* **90**, 3958–3962.
- Prasad, L., Sharma, S., Vandonselaar, M., Quail, J.W., Lee, J.S., Waygood, E.B., Wilson, K.S., Dauter, Z. & Delbaere, L.T. (1993) Evaluation of mutagenesis for epitope mapping. Structure of an antibody-protein antigen complex. *J. Biol. Chem.* **268**, 10705–10708.
- Pillet, L., Trémeau, O., Ducancel, F., Drevet, P., Zinn-Justin, S., Pinkasfeld, S., Boulain, J.C. & Ménez, A. (1993) Genetic engineering of snake toxins. Role of invariant residues in the structural and functional properties of a curaremimetic toxin, as probed by site-directed mutagenesis. *J. Biol. Chem.* **268**, 909–916.
- Trémeau, O., Lemaire, C., Drevet, P., Pinkasfeld, S., Ducancel, F., Boulain, J.C. & Ménez, A. (1995) Genetic engineering of snake toxins. The functional site of erabutoxin a, as delineated by site-directed mutagenesis, includes variant residues. *J. Biol. Chem.* **270**, 9362–9369.
- Endo, T. & Tamiya, N. (1991) Structure-function relationships of postsynaptic neurotoxins from snake venoms. In *Snake Toxins* (Harvey, A.L., ed.), pp 165–222. Pergamon Press, New York, USA.
- Corfield, P.W., Lee, T.J. & Low, B.W. (1989) The crystal structure of erabutoxin a at 2.0-Å resolution. *J. Biol. Chem.* **264**, 9239–9242.
- Bourne, P.E., Sato, A., Corfield, P.W., Rosen, L.S., Birken, S. & Low, B.W. (1985) Erabutoxin b. Initial protein refinement and sequence analysis at 0.140-nm resolution. *Eur. J. Biochem.* **153**, 521–527.

10. Zinn-Justin, S., Roumestand, C., Gilquin, B., Bontems, F., Menez, A. & Toma, F. (1992) Three-dimensional solution structure of a curarimimetic toxin from *Naja nigricollis* venom: a proton NMR and molecular modeling study. *Biochemistry* **31**, 11335–11347.
11. Le Goas, R., LaPlante, S.R., Mikou, A., Delsuc, M.A., Guittet, E., Robin, M., Charpentier, I. & Lallemand, J.Y. (1992) Alphacobratoxin: proton NMR assignments and solution structure. *Biochemistry* **31**, 4867–4875.
12. Yu, C., Bhaskaran, R., Chuang, L.C. & Yang, C.C. (1993) Solution conformation of cobrotoxin: a nuclear magnetic resonance and hybrid distance geometry-dynamical simulated annealing study. *Biochemistry* **32**, 2131–2136.
13. Brown, L.R. & Wütrich, K. (1992) Nuclear magnetic resonance solution structure of the alpha-neurotoxin from the black mamba (*Dendroaspis polylepis polylepis*). *J. Mol. Biol.* **227**, 1114–1135.
14. Ducancel, F., Boulain, J.C., Trémeau, O. & Ménez, A. (1989) Direct expression in *E. coli* of a functionally active protein A–snake toxin fusion protein. *Protein Eng.* **3**, 139–143.
15. Boyot, P., Pillet, L., Ducancel, F., Boulain, J.C., Trémeau, O. & Ménez, A. (1990) A recombinant snake neurotoxin generated by chemical cleavage of a hybrid protein recovers full biological properties [published erratum appears in *FEBS Lett.* (1990); **271** (1–2): 258]. *FEBS Lett.* **266**, 87–90.
16. Arnoux, B., Menez, R., Drevet, P., Boulain, J.C., Ducruix, A. & Ménez, A. (1994) Three-dimensional crystal structure of recombinant erabutoxin a at a 2.0 Å resolution. *FEBS Lett.* **342**, 12–14.
17. Zinn-Justin, S., Pillet, L., Ducancel, F., Thomas, A., Smith, J.C., Boulain, J.C. & Ménez, A. (1994) Engineering of protein epitopes: a single deletion in a snake toxin generates full binding capacity to a previously unrecognized antibody. *Protein Eng.* **7**, 917–923.
18. Ries-Kautt, M. & Ducruix, A. (1997) Inferences drawn from physico-chemical studies of crystallogenesis and the precrystalline stage. *Methods Enzymol.* **276**, 23–59.
19. Saludjian, P., Prange, T., Navaza, J., Ménez, R., Guilloteau, J.P., Ries-Kautt, M. & Ducruix, A. (1992) Structure determination of a dimeric form of erabutoxin b, crystallized from a thiocyanate solution. *Acta Crystallogr.* **B48**, 520–531.
20. Fourme, R., Dhez, P., Benoit, J.-P., Kahn, R., Dubuisson, J.-M., Besson, P. & Frouin, J. (1992) Bent crystal, bent multilayer optics on a multipole wiggler line for an X-ray diffractometer with an imaging plate detector. *Rev. Sci. Instrum.* **63**, 982–987.
21. Leslie, A.G.W. (1990) Molecular data processing. *Crystallogr. Comp.* **5**, 50–61.
22. Collaborative Computational Project, N. (1994) The CCP4 suite: programs for protein crystallography. *Acta Crystallogr.* **D50**, 760–763.
23. Brünger, A.T., Krukowski, A. & Erickson, J.W. (1990) Slow-cooling protocols for crystallography refinement by simulated annealing. *Acta Crystallogr.* **A46**, 585–593.
24. Brünger, A.T. (1992) Free R value: a novel statistical quantity for assessing the accuracy of crystal structures. *Nature* **355**, 472–475.
25. Lamzin, V.S. & Wilson, K.S. (1993) Automated refinement of protein models. *Acta Crystallogr.* **D49**, 129–147.
26. Navaza, G. (1994) AMoRe: an automated package for molecular replacement. *Acta Crystallogr.* **A50**, 157–163.
27. Laskowski, R.A., MacArthur, M.W., Moss, D.S. & Thornton, J.M. (1993) PROCHECK: a program to check the stereochemical quality of protein structures. *J. Appl. Crystallogr.* **26**, 283–291.
28. Read, R.J. (1986) Improved Fourier coefficients for map using phases from partial structures with errors. *Acta Crystallogr.* **A42**, 140–149.
29. Ménez, A., Bouet, F., Fromageot, P. & Tamiya, N. (1976) On the role of tyrosyl and tryptophanyl residues in the conformation of two snake neurotoxins. *Bulletin l'Inst. Pasteur* **74**, 57–64.
30. Ménez, A. (1977) *Marquage à l'iode et au tritium d'agents curarisants et cardiotoxiques. Etude de la conformation en solution des polypeptides toxiques extraits de venin de serpent.* Thèse d'Etat, Université Paris VII, France.
31. Hatanaka, H., Oka, M., Kohda, D., Tate, S., Suda, A., Tamiya, N. & Inagaki, F. (1994) Tertiary structure of erabutoxin b in aqueous solution as elucidated by two-dimensional nuclear magnetic resonance. *J. Mol. Biol.* **240**, 155–166.
32. Sibanda, B.L., Blundell, T.L. & Thornton, J.M. (1989) Conformation of beta-hairpins in protein structures. A systematic classification with applications to modelling by homology, electron density fitting and protein engineering. *J. Mol. Biol.* **206**, 759–777.
33. Ramachandran, G.N. & Sasisekharan, V. (1968) Conformation of polypeptides and proteins. *Advan. Protein Chem.* **23**, 283–437.
34. le Du, M.H., Marchot, P., Bougis, P.E. & Fontecilla-Camps, J.C. (1992) 1.9 Å resolution structure of fasciculin1, an anti-acetylcholinesterase toxin from green mamba snake venom. *J. Mol. Biol.* **267**, 22122–22130.
35. le Du, M.H., Housset, D., Marchot, P., Bougis, P.E., Navaza, J. & Fontecilla-Camps, J.C. (1996) Structure of fasciculin 2 from green mamba snake venom: evidence for unusual loop flexibility. *Acta Crystallogr.* **D52**, 87–92.
36. Bilwes, A., Rees, B., Moras, D., Ménez, R. & Ménez, A. (1994) X-ray structure at 1.55 Å of toxin gamma, a cardiotoxin from *Naja nigricollis* venom. Crystal packing reveals a model for insertion into membranes. *J. Mol. Biol.* **239**, 122–136.
37. Nicholls, A., Sharp, K.A. & Honig, B. (1991) Protein folding and association: insights from the interfacial and thermodynamic properties of hydrocarbons. *Proteins* **11**, 281–296.
38. Smith, J.L., Corfield, P.W., Hendrickson, W.A. & Low, B.W. (1988) Refinement at 1.4 Å resolution of a model of erabutoxin b: treatment of ordered solvent and discrete disorder. *Acta Crystallogr.* **A44**, 357–368.
39. Labhardt, A.M., Hunziker-Kwik, E.H. & Wütrich, K. (1988) Secondary structure determination for alpha-neurotoxin from *Dendroaspis polylepis polylepis* based on sequence-specific <sup>1</sup>H-nuclear-magnetic-resonance assignments. *Eur. J. Biochem.* **177**, 295–305.
40. Golovanov, A.P., Lomize, A.L., Arseniev, A.S., Utkin, Y.N. & Tsetlin, V.I. (1993) Two-dimensional <sup>1</sup>H-NMR study of the spatial structure of neurotoxin II from *Naja naja oxiana*. *Eur. J. Biochem.* **213**, 1213–1223.